Angle-Resolved Coherent Wave-Mixing using a 4 fs Ultra-Broad Bandwidth Laser

I. P. MERCER[1,*], T. WITTING[2], T. DRIVER[2], R. J. COGDELL[3], J.P. MARANGOS[2], J.W.G. TISCH[2]

[1] School of Physics, Centre for Synthesis and Chemical Biology, University College Dublin, Dublin 4, Ireland.
[2] Quantum Optics and Laser Science Group, Blackett Laboratory, Imperial College, London, UK.
[3] Institute of Molecular, Cell and Systems Biology, College of Medical, Veterinary and Life Sciences, University of Glasgow, Glasgow, UK.
*Corresponding author: ian.mercer@ucd.ie

Received XX Month XXXX; revised XX Month, XXXX; accepted XX Month XXXX; posted XX Month XXXX (Doc. ID XXXXX); published XX Month XXXX

We demonstrate Angle-Resolved Coherent (ARC) wave-mixing using 4 fs light pulses derived from a laser source that spans 550 to 1000 nm. We believe this to be the shortest pulse duration used to date in Coherent Multi-Dimensional Spectroscopy (CMDS). The marriage of this ultrabroad band, few-cycle coherent source with the ARC technique will permit new investigations of the interplay between energy transfers and quantum superposition states spanning 8200 cm^{-1}. We applied this configuration to measurements on the photosynthetic LL complex from Rps palustris in solution at ambient temperature. We observe bi-exponential population dynamics for energy transfer across 5500 cm^{-1} (0.65 eV), which we attribute to energy transfer from the Q_x transition of bacteriochlorophylls to the B850 pigment of the complex. For the first time we demonstrate that ARC maps can be recorded using a single laser pulse.

OCIS codes: *300.6530 Spectroscopy, ultrafast;* 300.6290 Spectroscopy, four-wave mixing; *270.1670 Coherent optical effects.*

http://dx.doi.org/10.1364/OL.99.099999

Life has evolved sophisticated molecular mechanisms and it remains challenging to reveal the connection between molecular function and structure with current techniques. A direct way to reveal what are sequential events is to conduct time-resolved measurements. An ideal technique would be non-invasive and sensitive to pertinent events in condensed phase molecules, proteins and semiconductors. Linear spectroscopic techniques such as optical absorption and fluorescence are non-invasive, but molecular dynamics acts to broaden spectral features and so limit the information gained from the condensed phase at ambient temperature. Significant progress is however being made using non-linear optical techniques collectively termed coherent multi-dimensional spectroscopy [1-15], and a wider applicability of these techniques may now be achieved by increasing mapped bandwidths and sensitivities. Recently, laser pulses as short as 10 fs [5] and 7 fs [9] have been used in coherent multi-dimensional spectroscopy.

We previously demonstrated a new coherent multi-dimensional spectroscopy, Angle-resolved Coherent (ARC) four wave-mixing, and we used this to reveal function in a photosynthetic protein [4]. With this approach, the selection of interaction frequencies by a molecular sample determines the angular distribution of the signal intensity and this is mapped using a camera array positioned in the optical far-field of the sample. Molecular quantum superposition states and energy transfers are mapped to orthogonal feature displacements and this permits a simultaneous characterization of their interplay in a single map. This occurs optically and no post-processing is required in principle. In theory, the technique should support ultra-short duration driving-pulses using an ultra-wide bandwidth [8]. However this has remained to be tested to date because the light source was restricted in bandwidth to 1500 cm^{-1}. Here we show that we can achieve a pulse duration of just 4 fs for the driving fields at the sample plane, using an ultra-wide laser spectrum spanning 8200 cm^{-1}, close to an octave.

The ARC apparatus is illustrated in figure 1(a). A diffractive optic (DO, 1mm thick silica, Holo/Or) generates four broadband driving beams from a single coherent input beam and an afocal telescope of unit magnification images three of these beams to a sample. The resulting signal field is projected to the optical far-field and directly onto a two-dimensional camera array (Mako G419-B NIR with 12 bit dynamic range). This arrangement has been modified to support the shortest possible pulse durations at the sample plane by translating the curved mirrors of the telescope apparatus using translation stages as opposed to using silica wedges for the control of relative pulse delays, thus eliminating higher order dispersion.

With reference to figure 1, in the absence of aberrations or misalignments, the direction of the signal field is given by [8]:

$$\begin{bmatrix} x' \\ y' \end{bmatrix}_S = \left(\frac{ck_g}{\omega_S} + \frac{\varphi}{2} \right) \begin{bmatrix} -1 \\ +1 \end{bmatrix} + \frac{\varphi}{\omega_S} \begin{bmatrix} \delta \\ \Delta \end{bmatrix} \quad (1)$$

where x' and y' are angles in the x-z and y-z planes respectively, c is the speed of light taking air as equivalent to vacuum, $k_g = 2\pi/d$ where d is the DO line spacing, $\delta = -\omega_3 + \omega_S$ is the difference in frequencies for a superposition state, and Δ is the energy transfer or reorganization energy, where ω_i is the interaction frequency and $i = 1, 2, 3, S$ for the three driving and signal fields, respectively, acting in the interaction time-ordering shown in figure 1(d). As illustrated in figure 1, the signal is directed to the remaining corner of a box formed by the three driving fields. Further deviations in the angle of signal emissions derive from the signal frequency (ω_S), molecular superposition states (δ) and energy transfers (Δ) as selected by the sample molecules from the ultra-broad bandwidth driving fields. Figure 1(d) shows a quantum interaction sequence where solid and dashed lines represent simultaneous quantum pathways for electronic excitation (green) and de-excitation (red) of a superposition state by a photon. State energies evolve independently during the evolution period t_{23}, as illustrated. For the condensed phase it can be useful to consider the evolution of a reduced density matrix in Liouville space for which real and conjugate field interactions combine in pairs for a molecular excitation (green) during t_{12} and de-excitation (red) during t_{3S} [3].

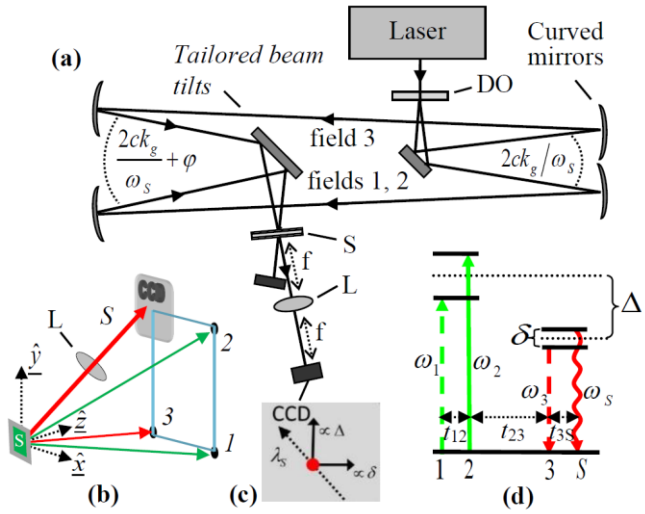

Fig. 1. Our ARC-4WM arrangement, showing: (a) driving fields selected from a diffractive optic (DO) imaged to the sample with a modified telescope; (b) laser and signal wave-vectors after the sample, S and showing a lens, L of focal length, f = 30 cm (singlet Bk7), and; (c) mapping to the camera array (see equation 1); (d) a representative field interaction sequence for the general case of exciting a quantum superposition state and for a delay of field 3.

To tailor the apparatus for a sensitivity to molecular state energies, the telescope is modified by introducing a relative tilt, φ between the driving field optical paths (in each of $\hat{x}$ and $\hat{y}$). This introduces an angle φ between the driving field group fronts at the sample. Consequently, a gain in spectral resolution leads to an unavoidable loss in time resolution due to a reduction in the overlap of group fronts at the sample. This trade-off is a manifestation of the uncertainty (or Fourier) principle and an analogous requirement pertains to two-dimensional Fourier transform spectroscopy (heterodyned four wave-mixing) for which the determination of an excitation frequency requires integrating over a delay between pulses.

The apparatus spectral and time resolution, is given by [8]:

$$dA = 4400\, N/\varphi W \quad (2)$$

$$\tau = 1.7\, \varphi W \quad (3)$$

where A (in cm^{-1}) is either δ in $\hat{x}$ or Δ in $\hat{y}$ for the pulse sequence in figure 1(d), τ (in fs) is the duration of the apparatus impulse response, where W (in mm) is the signal waist (intensity FWHM) at the sample for an instantaneous response i.e., taken to be $1/\sqrt{3}$ that of the driving fields, and $N \sim 1.2$ is the ratio of the signal divergence to that in the diffraction limit. This provides a measure of the spectral and time resolution from considering the optical point spread function at the detector and the overlap of group fronts between two driving fields at the sample.

For the present work, the apparatus is set for dA = 80 cm^{-1} and τ = 110 fs, which suits the characterization of molecular state energies as well as the dynamics of the LH2 protein. This is done by setting $\varphi = 2.3^o$ in each of $\hat{x}$ and $\hat{y}$ and by setting W = 1.6 mm. Alternatively the apparatus can be arranged to remove spectral resolution by setting φ = 0, for which τ = 0 (see equation 3) because the driving fields have zero relative group delay across beam [16]. In the presence of optical aberrations and misalignments it is not obvious, however, that the very shortest pulse durations should be reproduced at the sample. Here, we measure a pulse duration of just 4 fs at the sample plane.

The laser consists of a carrier-envelope phase-stabilized Ti:sapphire chirped pulse amplification system (Femtopower, Femtolasers) providing pulse energies of 2.5 mJ in a pulse duration of 28 fs at a repetition rate of 1 kHz. For these experiments, we focus a 1 mJ pulse from the laser into a 1 m long differentially pumped hollow core capillary for spectral broadening [17, 18]. The capillary is pressurised with up to 2.8 bar of neon at the exit side whilst the entrance side is maintained at vacuum. A double pass of a chirped mirror compressor (PC52, Ultrafast Innovations) compensates for positive dispersion introduced by air and material path between the capillary and the sample. The compression at the sample plane is monitored by intensity autocorrelation (see figure 2) and is tailored using a pair of BK7 wedges (OA325, Femtolasers) positioned before the ARC setup. The optical power is adjustable at the entrance to the ARC apparatus using broad-band polarizers (WP25MVIS, Thor Labs) and beam-splitters (OA157, Femtolasers) and for the following measurements the pulse energy was set to 6 μJ contained within the intensity FWHM of each driving field at the sample.

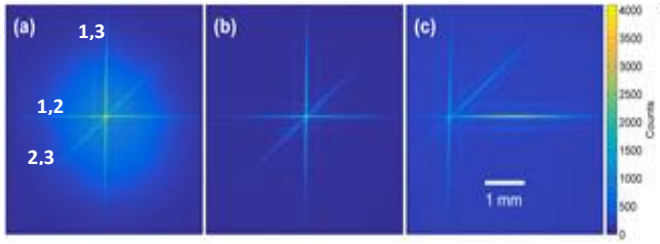

Fig. 2. Intensity autocorrelations of the driving fields at the sample plane, taken by imaging a BBO crystal placed at the sample plane to a CMOS array (AVT Guppy Pro F-503B with >30% of peak sensitivity in the range 240 - 780 nm, aligned to $\hat{x}$ and $\hat{y}$) with unit magnification: (a) including the second harmonic emission of each field; (b) blocking the second harmonic emission of each field; (c) as figure (b) but with field 3 delayed by 300 fs relative to fields 1 and 2 (see figure 1(d)).

Figure 2 shows intensity autocorrelation measurements imaged with unit magnification from a nonlinear optical crystal (5 micron thick BBO, cut for type I phase-matching), placed at the sample plane. A singlet lens of 15 cm focal length is used for this, positioned at 30 cm from both the sample plane and the camera array. The labelling of the beam correlations follows from figure 1(b).

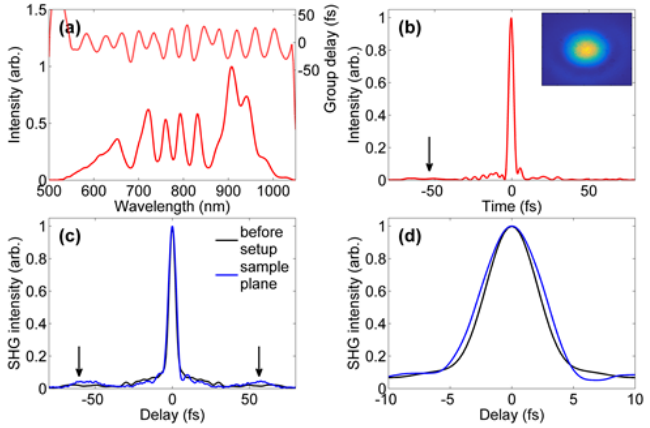

Fig. 3. Characterization of the laser source before the ARC setup and at the sample plane, showing the: (a) spectral intensity (lower trace) and spectral group delay (upper trace) measured by SEA-F-SPIDER before the ARC setup; (b) temporal intensity corresponding to figure (a), also showing the spatial beam profile at the input to the apparatus of width 2.8 mm FWHM, <1.2 times diffraction limited (inset); (c, d) intensity autocorrelation of the pulse profile before the ARC setup (black) as calculated from figure (b) and as measured at the sample plane (blue).

Figure 3(a) shows the intensity spectrum and the group delay measured before the ARC apparatus sampling the full beam using SEA-F-SPIDER [19]. The corresponding temporal intensity and group delay is shown in figure 3(b), for which the pulse duration is 3.7 fs FWHM (sech^2). Figures 3(c) and 3(d) show that the autocorrelation derived from SPIDER compares closely with the autocorrelation measured by averaging over the full beam width at the sample plane (see figure 2). The autocorrelation duration measured at the sample plane is 6.0 fs FWHM, corresponding to a pulse duration of 4.3 fs (Gauss) or 3.9 fs (sech^2).

ARC measurements were performed on the light harvesting LL complex from *Rhodopsuedomonas (Rps) palustris* [20]. Cells of *Rps palustris* 2.1.6 were grown anaerobically at low light intensity, as previously described [20], and the typical low light form of LH2 (LL LH2) was isolated and purified in the presence of the detergent LDAO [21]. The purified LL LH2 complex was stored at -20C in 0.1% LDAO, 20mM Tris HCl pH 8.0 until required.

Figure 4 shows ARC maps for which beam 3 is delayed relative to beams 1 and 2 for what we refer to as a transient grating (TG) sequence. Each map is taken with a single laser pulse. The laser spectrum is highly stable and this results in maps that are stable pulse-to-pulse. These maps are unfiltered in detection and shown on a logarithmic scale but without any additional processing. With reference to equation 1, the scale along the diagonal gives the wavelength of molecular emission, λ_S and orthogonal deviations from this derive from the excitation of quantum superposition states ($\propto \delta$) and from molecular energy transfer ($\propto \Delta$). This orthogonality in a single map permits a simultaneous characterization of the interplay of these mechanisms using a single laser pulse.

Three maxima are observed on the diagonal at zero delay resulting from the product of the light source and sample spectra. As the third field is delayed, symmetry about the diagonal is removed, leaving signal emission from pathways excited by the first and second fields only, as illustrated in figure 1(d). As the delay is increased, emission from the B800 ring diminishes as population is transferred from it to the B850 molecular ring via dipole-dipole coupling (FRET). At longest delays, emission derives only from B850 and this emission extends along $\hat{y}$ from the diagonal. In this limit, a vertical lineout intercepting λ_S on the diagonal relates to an excitation spectrum for emission at that wavelength. Emission is observed for λ_S > 950 nm at a level of ~1% of the main emission. Whilst this may be expected from a broad excited state emission, it may be that some features contain a contribution from excited state absorption into B850 and further work is required to characterise the dynamic range of the ARC technique.

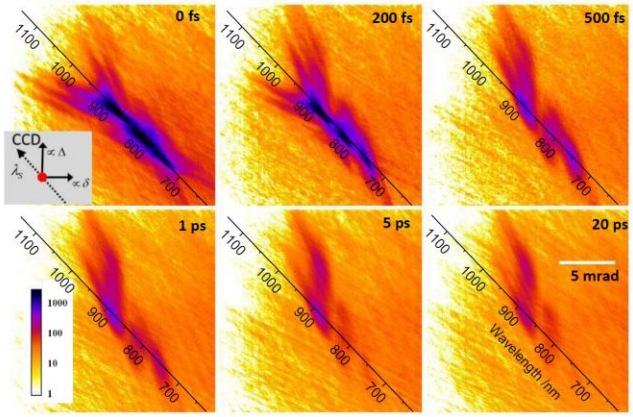

Fig. 4. Single laser pulse ARC maps of the LL complex from *Rps palustris*, for six TG delay times, unfiltered. Images are presented on a logarithmic scale but are otherwise shown as detected, with the intensity scale bar given in pixel count. The inset illustrates a signal deviation (see equation 1).

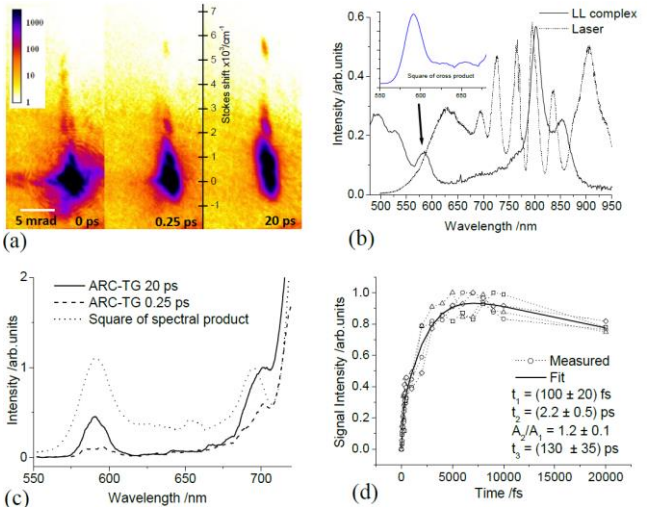

Fig. 5. ARC transient grating maps for the LL complex from *Rps palustris*, for the signal filtered for 852 nm and averaged over 800 pulses, showing: a) a feature emerging as a function of TG delay corresponding to Δ = 5500 cm^{-1} (0.65 eV), displayed in camera pixel count after background subtraction; b) the sample absorption and laser intensity spectra measured at the sample plane, inset with the square of the cross product of the two spectra; c) a comparison of this spectral cross-product with ARC-TG vertical lineouts, and; d) integrated signal intensity of the Δ = 5500 cm^{-1} feature shown for four consecutive TG scans (two with delay of field 2 and two with delay of field 3) and the resulting fit.

Figure 5 shows ARC TG maps using a spectral filter with transmission 852nm +/-5 nm positioned before the camera, in this way sensing emission from the B850 ring primarily. We observe a feature developing with TG delay that is separated from the diagonal by an angle, θ = 18.1 mrad in $\hat{y}$. From equation 1, $\Delta = (\omega_S/\varphi)\theta$ = 5500 cm^{-1} (0.65 eV) and this emission at 850 nm derives from excitation centred at 590 nm. Figure 5(b) shows the predicted TG excitation spectrum given by the square of the cross product of the absorption and laser spectra. As shown in figure 5(c), this predicted TG excitation spectrum is in good agreement with the measured vertical lineouts from figure 5(a) plotted against excitation wavelength, and so we conclude that this ARC feature derives from the 580 nm absorption feature. This is attributed to the Q_x transition of bacteriochlorophyll (Bchl) molecules that make up the two pigment rings (B800 and B850) of the complex [22].

Figure 5(d) plots the integrated intensity of the energy transfer feature as a function of TG delay. We observe a bi-exponential behaviour for the population transfer to the B850 ring with fitted population transfer times of t_1 = (100 ± 20) fs and t_2 = (2.2 ± 0.5) ps and broadly equal contributions ($A_2/A_1 \sim 1$). The 100 fs component constitutes an upper limit on the fast component of population transfer given the apparatus response time set to τ = 110 fs (see equation 3 and associated discussion). The two components of energy transfer are attributed to exciting the Q_x transition of Bchl's that directly populates the B850 ring and also indirectly populates it via the B800 ring [22]. In addition there is a long timescale population decay from the B850 ring, with t_3 = (130 ± 35) ps.

In conclusion, for the first time we demonstrate ARC wave-mixing using an ultra-broad bandwidth laser that spans 550 to 1000 nm (8200 cm^{-1}) and we measure a driving laser pulse duration of just 4 fs at the sample. This allows for studies of the interplay between energy transfers and molecular quantum superposition states spanning 8200 cm^{-1}. Specific to ARC wave-mixing, superposition states and energy transfers are characterized by orthogonal feature displacements contained within a single map. Along with our demonstration here of an ability to take an ARC map using a single laser pulse, this allows for the study of fragile samples that are otherwise damaged under bright light conditions. Also, for the currently proposed technique of ARC six wave-mixing (two-dimensional Raman) [8], this broad and coherent spectrum may provide for a simultaneous mapping of couplings between vibrations and overtones of up to 8200 cm^{-1}.

In the present work, the apparatus was set for an instrument energy and temporal resolution of 80 cm^{-1} and 110 fs respectively, in order to characterize the molecular state energies and dynamics of the photosynthetic LL complex from *Rps palustris*, in solution and at ambient temperature. For the first time, we characterize energy transfers across as much as 5500 cm^{-1} (0.65 eV). We observe bi-exponential dynamics for this highest energy transfer which we attribute to energy transferring into the B850 exciton from the Bacteriochlorophyll Q_x transitions of both B800 and B850. In further work, we look to characterise energy transfer into B800 and the contribution of excited state absorption to these dynamics. The ARC apparatus is flexible and can be configured to trade spectral for temporal resolution by aligning the driving fields to have zero relative group delay across the beam waist. This allows for observing quantum dynamics on timescales as fast as 4 fs in pump-probe or echo wave-mixing experiments, on surfaces or in bulk. The ARC apparatus is also flexible to the use of high pulse energies (~ mJ) and large beam waists (~ cm), and this is only limited by the dimensions of the present setup.

Funding. EPSRC grant EP/I032517/1; ERC ASTEX project 290467 and; UCD Physics Equipment Fund 2014. Work at the University of Glasgow was supported as part of the Photosynthetic Antenna Research Center (PARC), an Energy Frontier Research Center funded by the U.S. Department of Energy, Office of Science, Basic Energy Sciences under Award #DE-SC0001035.

References

1. J. D. Hybl, A. A. Ferro, and D. M. Jonas, J Chem Phys **115**, 6606-6622 (2001).
2. V. I. Prokhorenko, A. Halpin, and R. J. D. Miller, Opt Express **17**, 9764-9779 (2009).
3. S. Mukamel, *Principles of nonlinear optical spectroscopy* (Oxford University Press, 1995).
4. I. P. Mercer, Y. C. El-Taha, N. Kajumba, J. P. Marangos, J. W. G. Tisch, M. Gabrielsen, R. J. Cogdell, E. Springate, and E. Turcu, Phys Rev Lett **102**, 057402 (2009).
5. M. Maiuri, J. Réhault, A.-M. Carey, K. Hacking, M. Garavelli, L. Lüer, D. Polli, R. J. Cogdell, and G. Cerullo, The Journal of Chemical Physics **142**, 212433 (2015).
6. D. M. Monahan, L. Whaley-Mayda, A. Ishizaki, and G. R. Fleming, The Journal of Chemical Physics **143**, 065101 (2015).
7. A. Remorino, and R. M. Hochstrasser, Accounts Chem Res **45**, 1896-1905 (2012).

8. I. P. Mercer, Phys Rev A **82**, 043406 (2010).
9. X. Ma, J. Dostál, and T. Brixner, Opt Express **24**, 20781-20791 (2016).
10. J. C. Wright, Chem Phys Lett **662**, 1-13 (2016).
11. R. D. Mehlenbacher, T. J. McDonough, N. M. Kearns, M. J. Shea, Y. Joo, P. Gopalan, M. S. Arnold, and M. T. Zanni, The Journal of Physical Chemistry C **120**, 17069-17080 (2016).
12. H. Frostig, T. Bayer, N. Dudovich, Y. C. Eldar, and Y. Silberberg, Nat Photon **9**, 339-343 (2015).
13. K. J. Karki, J. R. Widom, J. Seibt, I. Moody, M. C. Lonergan, T. Pullerits, and A. H. Marcus, Nature communications **5** (2014).
14. K. L. Koziol, P. J. Johnson, B. Stucki-Buchli, S. A. Waldauer, and P. Hamm, Curr Opin Struc Biol **34**, 1-6 (2015).
15. M. Thämer, L. De Marco, K. Ramasesha, A. Mandal, and A. Tokmakoff, Science **350**, 78-82 (2015).
16. A. A. Maznev, T. F. Crimmins, and K. A. Nelson, Opt Lett **23**, 1378-1380 (1998).
17. F. Frank, C. Arrell, T. Witting, W. Okell, J. McKenna, J. Robinson, C. Haworth, D. Austin, H. Teng, and I. Walmsley, Rev Sci Instrum **83**, 071101 (2012).
18. J. Robinson, C. Haworth, H. Teng, R. Smith, J. Marangos, and J. Tisch, Applied Physics B **85**, 525-529 (2006).
19. T. Witting, F. Frank, C. A. Arrell, W. A. Okell, J. P. Marangos, and J. W. G. Tisch, Opt Lett **36**, 1680-1682 (2011).
20. M. B. Evans, A. M. Hawthornthwaite, and R. J. Cogdell, Biochimica et Biophysica Acta (BBA)-Bioenergetics **1016**, 71-76 (1990).
21. T. H. Brotosudarmo, R. Kunz, P. Böhm, A. T. Gardiner, V. Moulisová, R. J. Cogdell, and J. Köhler, Biophys J **97**, 1491-1500 (2009).
22. R. E. Blankenship, *Molecular mechanisms of photosynthesis* (Wiley, 2014).

References including titles

1. Hybl, J.D., A.A. Ferro, and D.M. Jonas, *Two-dimensional Fourier transform electronic spectroscopy.* Journal of Chemical Physics, 2001. **115**(14): p. 6606-6622.
2. Prokhorenko, V.I., A. Halpin, and R.J.D. Miller, *Coherently-controlled two-dimensional photon echo electronic spectroscopy.* Optics Express, 2009. **17**(12): p. 9764-9779.
3. Mukamel, S., *Principles of nonlinear optical spectroscopy*. 1995: Oxford University Press.
4. Mercer, I.P., et al., *Instantaneous Mapping of Coherently Coupled Electronic Transitions and Energy Transfers in a Photosynthetic Complex Using Angle-Resolved Coherent Optical Wave-Mixing.* Physical Review Letters, 2009. **102**(5): p. 057402.
5. Maiuri, M., et al., *Ultra-broadband 2D electronic spectroscopy of carotenoid-bacteriochlorophyll interactions in the LH1 complex of a purple bacterium.* The Journal of Chemical Physics, 2015. **142**(21): p. 212433.
6. Monahan, D.M., et al., *Influence of weak vibrational-electronic couplings on 2D electronic spectra and inter-site coherence in weakly coupled photosynthetic complexes.* The Journal of Chemical Physics, 2015. **143**(6): p. 065101.
7. Remorino, A. and R.M. Hochstrasser, *Three-Dimensional Structures by Two-Dimensional Vibrational Spectroscopy.* Accounts of Chemical Research, 2012. **45**(11): p. 1896-1905.
8. Mercer, I.P., *Angle-resolved coherent optical wave mixing.* Physical Review A, 2010. **82**(4): p. 043406.
9. Ma, X., J. Dostál, and T. Brixner, *Broadband 7-fs diffractive-optic-based 2D electronic spectroscopy using hollow-core fiber compression.* Optics Express, 2016. **24**(18): p. 20781-20791.
10. Wright, J.C., *Analytical chemistry, multidimensional spectral signatures, and the future of coherent multidimensional spectroscopy.* Chemical Physics Letters, 2016. **662**: p. 1-13.
11. Mehlenbacher, R.D., et al., *Polarization-Controlled Two-Dimensional White-Light Spectroscopy of Semiconducting Carbon Nanotube Thin Films.* The Journal of Physical Chemistry C, 2016. **120**(30): p. 17069-17080.
12. Frostig, H., et al., *Single-beam spectrally controlled two-dimensional Raman spectroscopy.* Nat Photon, 2015. **9**(5): p. 339-343.
13. Karki, K.J., et al., *Coherent two-dimensional photocurrent spectroscopy in a PbS quantum dot photocell.* Nature communications, 2014. **5**.
14. Koziol, K.L., et al., *Fast infrared spectroscopy of protein dynamics: advancing sensitivity and selectivity.* Current opinion in structural biology, 2015. **34**: p. 1-6.
15. Thämer, M., et al., *Ultrafast 2D IR spectroscopy of the excess proton in liquid water.* Science, 2015. **350**(6256): p. 78-82.
16. Maznev, A.A., T.F. Crimmins, and K.A. Nelson, *How to make femtosecond pulses overlap.* Optics Letters, 1998. **23**(17): p. 1378-1380.
17. Frank, F., et al., *Invited review article: technology for attosecond science.* Review of Scientific Instruments, 2012. **83**(7): p. 071101.
18. Robinson, J., et al., *The generation of intense, transform-limited laser pulses with tunable duration from 6 to 30 fs in a differentially pumped hollow fibre.* Applied Physics B, 2006. **85**(4): p. 525-529.
19. Witting, T., et al., *Characterization of high-intensity sub-4-fs laser pulses using spatially encoded spectral shearing interferometry.* Optics Letters, 2011. **36**(9): p. 1680-1682.
20. Evans, M.B., A.M. Hawthornthwaite, and R.J. Cogdell, *Isolation and characterisation of the different B800–850 light-harvesting complexes from low-and high-light grown cells of Rhodopseudomonas palustris, strain 2.1. 6.* Biochimica et Biophysica Acta (BBA)-Bioenergetics, 1990. **1016**(1): p. 71-76.
21. Brotosudarmo, T.H., et al., *Single-molecule spectroscopy reveals that individual low-light LH2 complexes from Rhodopseudomonas palustris 2.1. 6. have a heterogeneous polypeptide composition.* Biophysical journal, 2009. **97**(5): p. 1491-1500.
22. Blankenship, R.E., *Molecular Mechanisms of Photosynthesis*. 2nd ed. 2014: Wiley.